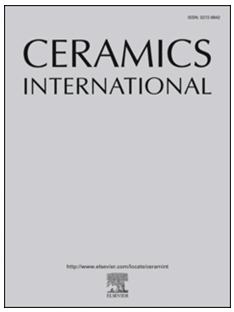

Electrochemical and structural study on cycling performance of γ-LiV_2O_5 cathode

Miloš Milović, Milica Vujković, Dragana Jugović, Miodrag Mitrić

PII: S0272-8842(21)00679-9

DOI: https://doi.org/10.1016/j.ceramint.2021.03.016

Reference: CERI 28081

To appear in: *Ceramics International*

Received Date: 25 January 2021

Revised Date: 3 March 2021

Accepted Date: 6 March 2021

Please cite this article as: M. Milović, M. Vujković, D. Jugović, M. Mitrić, Electrochemical and structural study on cycling performance of γ-LiV_2O_5 cathode, *Ceramics International*, https://doi.org/10.1016/j.ceramint.2021.03.016.

Electrochemical and structural study on cycling performance of γ-LiV_2O_5 cathode

Miloš Milović[1,*], Milica Vujković[2], Dragana Jugović[1] and Miodrag Mitrić[3]

[1] Institute of Technical Sciences of SASA, Belgrade, Serbia

[2] Faculty of Physical Chemistry, University of Belgrade, Belgrade, Serbia

[3] Vinča Institute of Nuclear Sciences – National Institute of the Republic of Serbia, University of Belgrade, Belgrade, Serbia

Keywords

Li-ion batteries, cathode materials, LiV_2O_5, gamma phase, bond valence model

Abstract

Electrochemical and structural properties of LiV_2O_5 cathode were investigated. Obtained by solid state reaction at high temperature the material crystallized as gamma polymorph phase, γ-LiV_2O_5. The gamma structure provides two crystallographic sites to accommodate lithium ions, Li1 and Li2 position. Lithium insertion at these two sites occurs at two respective voltages versus lithium metal: ~3.6 V (Li1) and ~2.4 V (Li2). Intercalation at Li1 position is reversible in both organic and aqueous electrolyte and provides stable cycling performance at the high voltage. On the contrary, sluggish insertion/removal of Li^+ at Li2 sites causes unstable performance and significant storage capacity fade at lower voltages. Lithium diffusion 3d landscape was

determined by bond valence calculations applied on the γ-LiV_2O_5 phase, as well as on the metastable phases of γ'-V_2O_5 and ζ-$Li_2V_2O_5$ that exist at high and low voltages respectively. The model was proposed based on inactivity of Li2 position of the metastable ζ-$Li_2V_2O_5$ phase which provides explanation for the observed storage capacity loss at low voltages.

Graphical abstract

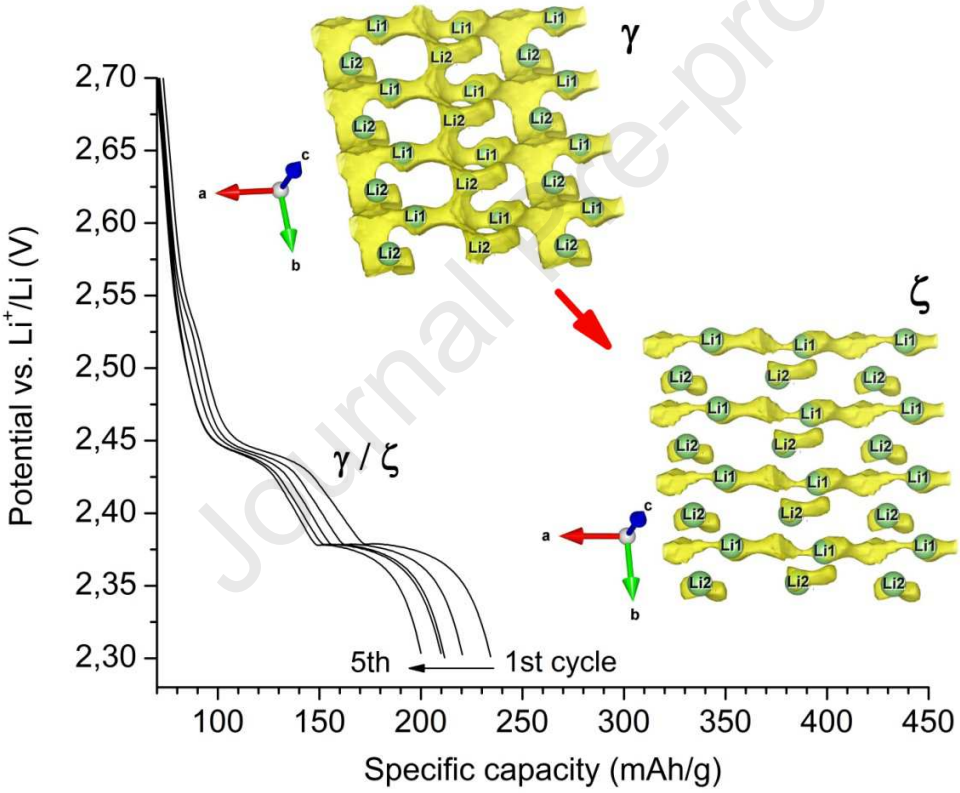

1. Introduction

Numerous investigations have been aimed towards application of vanadium pentoxide α-V_2O_5 as a cathode in rechargeable batteries, ever since electrochemical intercalation of lithium in this oxide has been discovered [1]. The electrochemical lithium insertion/extraction corresponds to the reaction:

$$xe^- + xLi^+ + V_2O_5 \leftrightarrow Li_xV_2O_5, \qquad (1)$$

where $Li_xV_2O_5$ can adopt various crystal modifications depending on lithium concentration and temperature. At the room temperature, single α-$Li_xV_2O_5$ phase exists for lithium content between $0<x<0.1$, ε-$Li_xV_2O_5$ for $0.35<x<0.7$ and δ-$Li_xV_2O_5$ for $0.9<x<1$ [2]. Since α, ε and δ phases are structurally very similar to each other and to the parent α-V_2O_5 phase, all structural changes in the range $0<x<1$ are reversible. In this range, lithium intercalation induce puckering of $(V_2O_5)_n$ layers with an increase of interlayer spacing, but V_2O_5 skeleton remains more-less unchanged. If, however, more than one lithium per formula is intercalated, irreversible structural change occurs resulting in the formation of the γ-$Li_xV_2O_5$ phase which exists in $1<x<1.8$ domain of the reaction (1) [3]. Complete deintercalation of γ-$Li_xV_2O_5$ leads to a metastable γ'-V_2O_5 with very similar structural characteristics (it keeps memory on the structure of original lithiated γ) [4–6]. The γ-$Li_xV_2O_5$ phase has a mixed valence state of vanadium V^{5+}/V^{4+} and high puckering of $(V_2O_5)_n$ layers (compared to α, ε and δ) which induces the enhancement of the cell potential. On the other hand, $(V_2O_5)_n$ interlayer distance is increased in γ-$Li_xV_2O_5$ when compared to pure α-V_2O_5 (5.33 against 4.37 Å) [7], thus facilitating lithium diffusion between the layers. The resulting potential of ~3.6 V, together with the capability of insertion more than one lithium ion per formula unit

makes gamma phase very interesting for potential cathode application in Li-ion batteries. It led researchers to directly synthesize and investigate γ-LiV_2O_5.

Electrochemical characteristics of γ-$Li_xV_2O_5$ ($x \approx 1$) were examined in the full $0<x<2$ range of lithium intercalation [8]. Deintercalation of lithium from γ-LiV_2O_5 at oxidation potentials larger than 3.5 V ($x \approx 0.4$) results in the formation of a new γ'-phase; at a potential of 3.65 V complete deintercalation was achieved, giving rise to a new form of vanadium pentoxide, γ'-V_2O_5. Reversible transformation between γ and γ' phase provides very stable cathode performance of γ-$Li_xV_2O_5$ in the $0<x<1$ range. After prolonged cycling in this region, in the voltage range between 4-3V, only negligible capacity fade was observed [9,10]. Utilization of high capacities is enabled by the insertion of the second lithium at the lower potentials, >2.5 V, but it induces, however, considerable stability issues. Initial high capacities of around 250 mAh/g for γ-$Li_xV_2O_5$ nanorods quickly diminish after several cycles of charge/discharge in the range 4-1.5V [11–13]. The capacity loss is ascribed to irreversible transformation of γ-$Li_xV_2O_5$ to a new metastable ζ-$Li_xV_2O_5$ polymorph at a lithium concentrations higher than $x>1.4$ [14]. Therefore, both insertion and extraction of lithium from γ-LiV_2O_5 leads to formation of the new metastable phases, lithium rich ζ and lithium poor γ' phase, respectively. All three phases belong to the same orthorhombic Pnma space group and have similar lattice parameters [8]. Still, (de)intercalation processes that occur at high (γ↔γ' conversion) and low voltages (γ↔ζ) noticeably differ in terms of the achieved capacity retention, with no apparent reason. Aside from the inherent structural properties, stability of a cathode is largely affected also by its microstructural characteristics. Nano-sized powders are known to provide higher storage capacities at higher rates, but generally for the cost of a lesser stability [15]. So, in this study, well-crystallized γ-LiV_2O_5 has been synthesized via solid state reaction at high temperatures. Electrochemical performances of thus

obtained micron size powder were investigated at high and low voltages in both organic and aqueous electrolyte. For the analysis of the structure-to-cathode property relations bond valence method have been utilized.

2. Experimental

For the synthesis of starting LiV_2O_5, stoichiometric amounts of Li_2CO_3 (Alfa Aesar, ≥99%) and V_2O_5 (Sigma-Aldrich, ≥99.6%) were mixed and thoroughly ground, then pelletized under 0.15 GPa and calcined for 2h at the temperature of 700 °C in a flowing, slightly reductive atmosphere of Ar + 10% H_2. Formation of LiV_2O_5 therefore goes with the solid state reaction as follows:

$$½Li_2CO_3 + V_2O_5 \rightarrow LiV_2O_5 + ½CO_2 + ¼O_2. \quad (2)$$

The X-ray powder diffraction measurement was performed on a Philips PW 1050 X-ray powder diffractometer using Ni-filtered Cu Kα radiation and Bragg-Brentano focusing geometry. The diffraction intensity was recorded in the 2θ range of 10–120° with a step size of 0.02° and a counting time of 15 s per step. The Rietveld structural refinement was performed with FullProf computer program in WinPLOTR environment [16]. For bond valance sum (BVS) calculations 3DBVSMAPPER [17] software was used. Morphology of the powder was examined by the means of scanning electron microscopy (SEM, Phenom ProX). The particle size distribution (PSD) was determined by a laser-diffraction-based particle size analyzer, Mastersizer 2000 (Malvern Instruments Ltd., UK). The Fourier transform infrared (FTIR) spectra of the sample was recorded in ambient conditions at 400-1200 cm^{-1} range with a Nicolet IS 50 FT-IR Spectrometer operating in the ATR mode and the measuring resolution of 4 cm^{-1} with 32 scans.

The electrochemical measurements were conducted by using Vertex.One potentiostat/galvanostat (Ivium Technologies). Galvanostatic charge/discharge tests were carried out in a closed, argon-

filled two-electrode cell with metallic Li as a counter electrode and 1M solution of $LiClO_4$ (Fluka, p.a.) in PC (propylene carbonate, Sigma-Aldrich 99.7%) as an electrolyte. Cyclic voltammetry (CV) measurements were performed in a three-electrode cell with platinum as a counter and SCE (saturated calomel electrode, SI Analytics) as a reference electrode; 6M solution of $LiNO_3$ (Alfa Aesar 99%) in H_2O was used as an electrolyte. Working electrode for both galvanostatic and CV measurements consisted of the active material, carbon black and poly-vinylidenefluoride (PVDF, Sigma-Aldrich) mixed in 75:20:5 weight ratio and deposited on a platinum foil from the slurry prepared in N-methyl-2-pyrrolidone (Sigma-Aldrich 99%).

3. Results and discussion

3.1. Structure

As confirmed by X-ray diffraction (Figure 1a), the prepared oxide LiV_2O_5 crystallized as γ polymorph phase and was refined accordingly in orthorhombic *Pnma* space group (no. 62) within the structure where each Li^+, V^{4+} and V^{5+} cation occupy one and O^{2-} anions occupy five different 4c crystallographic positions [x,0.25,z] as presented in Table 1. The previously reported unit cell parameters and atomic positions of the given phase [18] were used as a starting point for the Rietveld refinement. Polyhedral representation of the structure of γ-LiV_2O_5 is given in Figure 1b; it consists of layered $(V_2O_5)_n$ framework where altering corner and edge sharing $(V^{4+})O_5$ and $(V^{5+})O_5$ hexahedrons (triangular bipyramids exactly – very close to square pyramids, see Figure 1b) form layers in a-b plane thus providing deformed octahedral interlayer positions for lithium ions. Edge shared LiO_6 octahedrons form linear chains along b-direction which, as one might suspect, favors lithium diffusion along this direction in a similar manner as in olivine-$LiFePO_4$ (the same trend of LiO_6 connectivity in the orthorhombic space group no. 62 [19]). Since V^{4+} and

V^{5+} have different X-ray scattering factors and occupy two distinct crystallographic sites, V1(V^{4+}) and V2(V^{5+}), during the refinement procedure both cation oxidation states and occupancies on these sites were altered. The minimal R-factors were obtained when V^{4+} and V^{5+} fully occupy designated sites. This serves as confirmation that the average valence of vanadium in the prepared powder corresponds to the aimed 4.5, as stoichiometry dictates. The X-ray diffractogram reveals preferred orientation of the powder normal to (002) direction, which was also included in the refinement, and could be related to the layered structure of γ-LiV_2O_5 with the layers normal to c-axis. The value of preferred orientation parameter G1<1 suggests platy habit in the sample [20] and is in agreement with the appearance of the powder under electron microscope, as displayed in the inset of Figure 1a. SEM along with PSD analysis (Figure S1) reveals wide particle size distribution of the powder which consists of large number of smaller particles (average size of ~0.5 µm) and smaller number of large agglomerates with layered microstructure (average size of ~8 µm). All particles are polycrystalline. The average crystallite size was refined to 89 nm with the significant standard deviation value (Table 1) which suggests highly anisotropic crystallite growth. The obtained model of crystallite shape (Figure 1c) indicates a platy habit in the a-b plane as well and provides explanation for the preferred orientation of the powder.

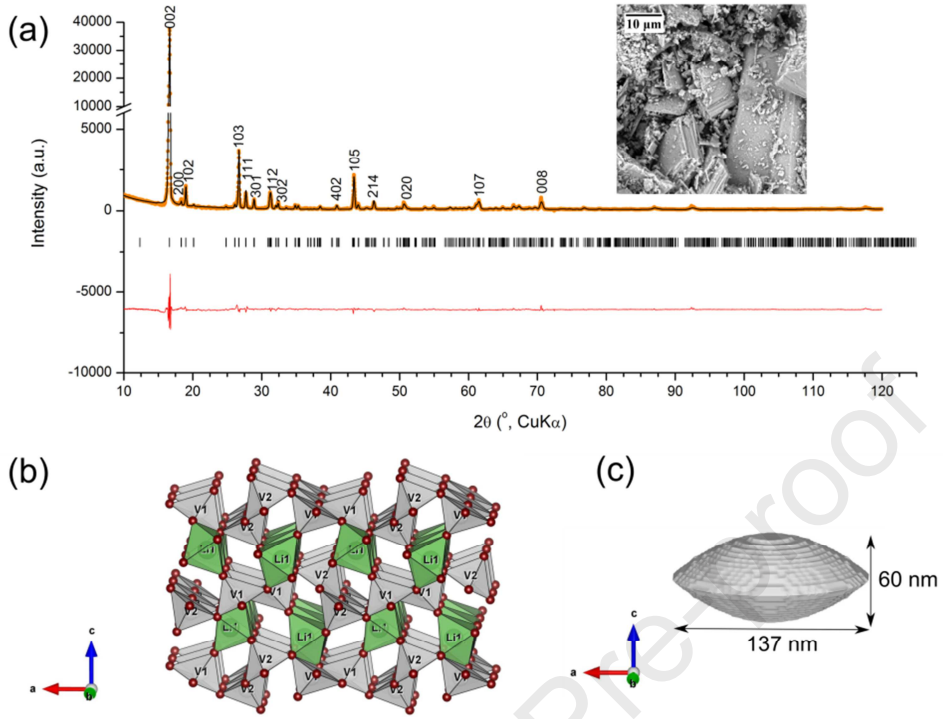

Figure 1. The observed (orange dots), calculated (black line) and difference (bottom red line) X-ray diffraction data taken at room temperature (a) and SEM micrograph of the γ-LiV_2O_5 powder (inset of a); vertical markers below the diffraction patterns indicate positions of possible Bragg reflections for the orthorhombic γ-LiV_2O_5. Crystal structure of γ-LiV_2O_5 (b). Refined model of the crystallites (c).

Table 1. Refined lattice, structural and microstructural parameters of the γ-LiV_2O_5.

Space group		P n m a				
Lattice parameters (Å)		a = 9.6995(7)		Preferred orientation		G1 = 0.4357(5)
		b = 3.6075(2)		Mean crystallite size (Å)		= 887(222)
		c = 10.6865(2)		Strain (%)		= 0.1221(1)
Cell volume (Å^3)		V = 373.93(4)				
Atomic position	Oxidation state	Wyckoff symbol	Fractional coordinates			$B_{overall}$ (Å^2)
			x	y	z	
Li1	Li1+	4c	0.173(2)	0.25	0.215(2)	2.09(3)
V1	V4+	4c	0.3735(6)	0.25	0.4979(3)	
V2	V5+	4c	0.0665(7)	0.25	0.6020(2)	
O1	O2-	4c	0.2464(19)	0.25	0.6308(6)	

O2	O2-	4c	0.4715(16)	0.25	0.7771(6)
O3	O2-	4c	0.2848(16)	0.25	0.3767(7)
O4	O2-	4c	0.5803(17)	0.25	0.4620(7)
O5	O2-	4c	0.4358(17)	0.25	0.0422(6)
R_{wp} factor (%) = 19.5					

Figure 2 shows FTIR spectrum of the as-synthesized γ-LiV_2O_5. In the vibrational spectra of all lithium vanadium oxides (δ, ε, γ) as well as in the spectrum of pure vanadium pentoxide (α), the most prominent are the modes of VO_5 group [21]. In the high frequency region (800-1200 cm^{-1}) gamma phase LiV_2O_5 has characteristic two strong bands at ~1000 and ~950 cm-1 (with the first one comprising of two merged bands) originating from V═O stretching vibrations [12,21,22]. In the intermediate frequency region (400-800 cm^{-1}) gamma LiV_2O_5 has as the most dominant one wide band consisting of several overlapping bands at around 720, 585, 540, 443 cm^{-1} etc, all originating from V─O─V bending vibrations as suggested in [21–23].

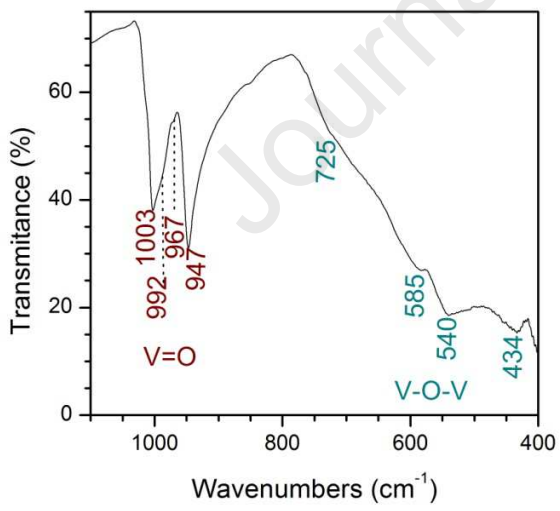

Figure 2. FTIR spectrum of the prepared γ-LiV_2O_5.

3.2. Electrochemistry

The prepared γ-LiV_2O_5 powder has been tested as cathode in Li-ion cell by galvanostatic charge-discharge cycling in organic electrolyte. The galvanostatic tests were performed at the room temperature in 4.0-2.3 V voltage range. From the obtained chronopotentiometric curves at the given current rate, the specific capacities were calculated using the mass of the active material only – mass of carbon is subtracted from loading. The current rates are presented in *c/n* units, where *c* is a 1-electron theoretical capacity of the material (which is 142 mAh/g for LiV_2O_5) and *n* is a discharge time given in hours needed for a complete discharge. The typical discharge profile of the material at various rates is shown in Figure 3. The profile is distinguished by two regions at high and low voltages. At the very beginning of discharge there is a biphasic domain of flat voltage at 3.6 V which corresponds to coexistence of delithiated γ'[4] and lithiated γ phase. It is followed by gradual slope of voltage which corresponds to solid solution insertion of Li^+ into γ host (monophasic γ region). During discharge, lithium first occupies octahedral Li1 crystallographic sites in γ' and subsequently in γ phase. When all available octahedral sites are occupied, γ structure provides another position – a tetrahedral site [8] – where lithium goes to. The new tetrahedral site has a different crystal field and therefore a different voltage of lithium insertion (low voltage region). At low voltages, lithium first intercalates in tetrahedral positions of γ host in a solid solution process at ~2.44 V and when certain lithium concentration is reached ($x \approx 1.4$) γ phase transforms to a new ζ phase [8,14]. The last plateau at 2.37 V therefore corresponds to biphasic γ/ ζ equilibrium.

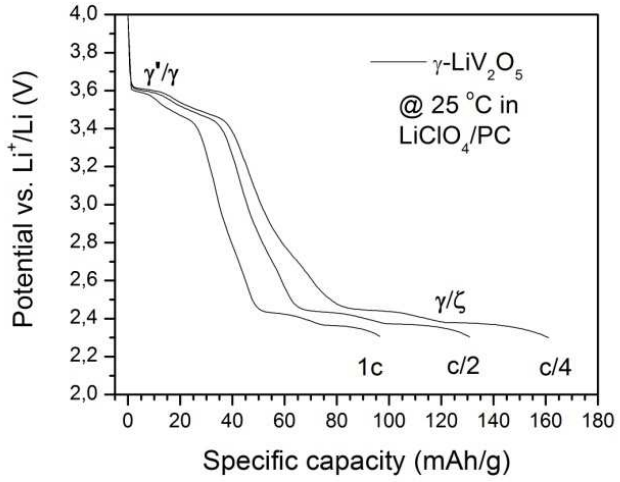

Figure 3. Discharge profiles of the γ-LiV_2O_5 at various rates.

However, the cycling performance does not prove to be stable in the given voltage range of 4.0-2.3 V. As shown in Figure 4a the obtained capacities were fading from the very first cycles and capacity decrease is particularly notable in the low voltage region (inset of Figure 4a). The observed behavior suggests that lithium insertion in tetrahedral sites and subsequent conversion of γ to ζ phase is mostly irreversible. This assumption is also supported by the charge/discharge profile discrepancy as evidenced in the original chronopotentiometric curves (Figure 4c): the low voltage region of charge profile is reduced when compared to discharge at the given current rate. On the other hand, in the high voltage region it appears that intercalation of lithium at octahedral sites and conversion of γ' to γ is completely reversible. Galvanostatic testing of another ("fresh") electrode provides very stable cycling performance in the 4-3 V voltage range (Figure 4b) with uniform charge and discharge profiles (Figure 4d).

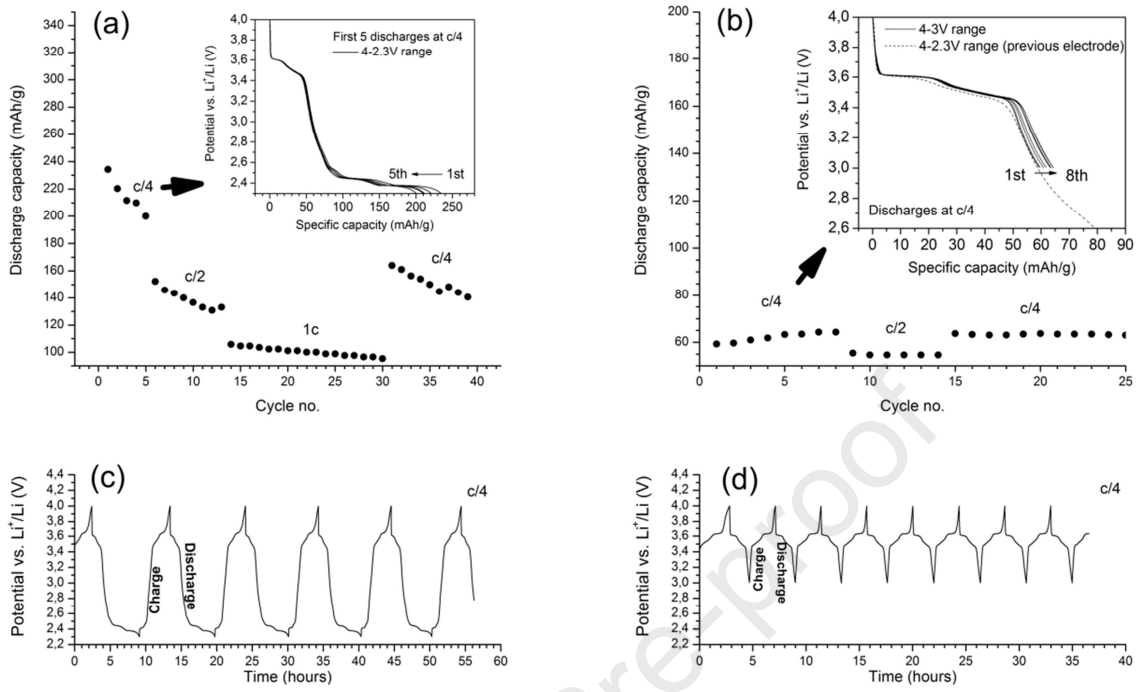

Figure 4. Cycling stability of the γ-LiV_2O_5 in 4-2.3 V (a) and 4-3 V voltage range (b) with the evolution of discharge profiles shown as inset and corresponding chronopotentiometric curves in 4-2.3 V (c) and 4-3 V voltage range (d). Testing was performed in $LiClO_4$/PC electrolyte at ambient temperature.

Redox behavior of the synthesized gamma phase was also evaluated by the cyclic voltammetry measurements in an aqueous electrolyte, with the compatible results and similar conclusions. The material showed the electrochemical activity caused by the V^{5+}/V^{4+} redox couple with two prominent pair of peaks at high and low voltages as displayed in Figure 5a. In high voltage region, there is a sharp reduction (discharge) peak at 0.40 V vs. SCE (I) that partially overlaps with a broader peak at 0.29 (II), corresponding to biphasic γ'/γ and monophasic γ lithium intercalation at octahedral sites, respectively. At lower voltages there are two more reduction peaks: a broad peak at -0.83 V vs. SCE (IV) with a noticeable shoulder at -0.75 (III). The last two

peaks (III & IV) – attributed to intercalation of lithium into tetrahedral sites of γ and subsequently ζ – appear to be unstable on cycling in a similar fashion as in organic electrolyte in the low voltage region. On the contrary, peaks at high voltages (I & II) provide excellent rate (Figure 5b) and stability performance (Figure 5b inset).

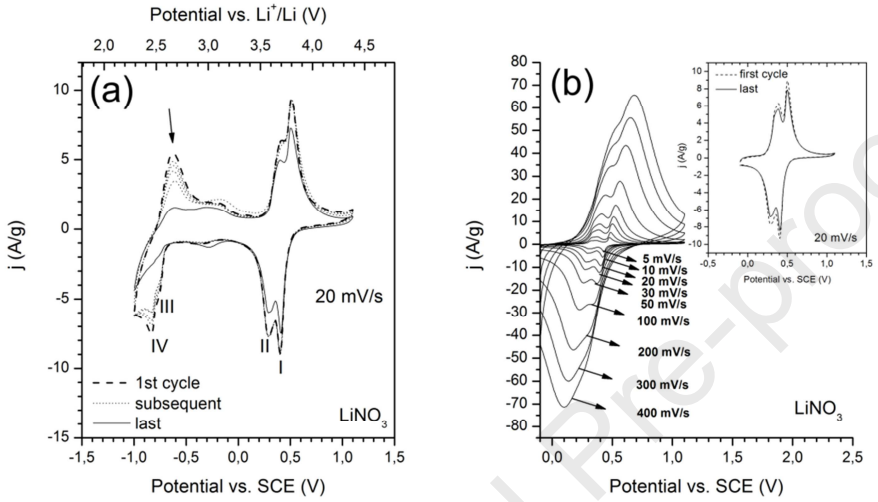

Figure 5. Cyclic voltammograms of the γ-LiV_2O_5 in $LiNO_3/H_2O$ electrolyte: voltage range from -1 to 1 V vs. SCE (a) and from -0.1 to 1 V vs. SCE (b). The potential vs. Li (top x-axis of a) is calculated from the measured potential vs. SCE (bottom x-axis of a) on the basis of reference tables for the standard electrode potentials in aqueous solutions vs. NHE [24]. Inset of b: CV profile before and after rate performance testing.

Ex situ X-ray diffraction measurements performed on cycled electrodes in a discharged state confirm that the mechanism of phase transformation does not differ in aqueous and organic electrolyte. Figure S2 reveals that the layered skeleton is preserved upon lithium intercalation, with the slight reduction of interlayer spacing, as evidenced by the shift of 002 reflection to higher angles, due to the formation of the ζ phase. The results of electrochemical measurements in both organic and aqueous electrolyte indicate sluggish reaction of intercalation in the low

voltage region when lithium occupies Li2 tetrahedral positions in γ and subsequently in ζ phase (when γ transforms to ζ). On the other side, intercalation at octahedral Li1 positions in the high voltage region appears perfectly feasible at the given rate conditions. The cause of evidenced performance differences at high and low voltages therefore must lie in the crystallographic differences of these two sites, Li1 and Li2. Let's take a closer look.

3.3. Bond valence

For the crystal analysis of the structures of interest bond valence method have been utilized. The method is based on the *valence sum rule* derived from the Pauling's electrostatic valence principle (no. 2) [25] that the sum of bond valences S_{ij} around atom (ion) *i* is equal to its valence V_i:

$$V_i = \sum_j S_{ij} = \sum_j e^{\frac{r_0 - d_{ij}}{b}}, \qquad (3)$$

where the sum goes over all neighboring atoms *j* of the atom *i* and each bond valence S_{ij} is inversely correlated with the bond length d_{ij} between atom *j* and atom *i* through a set of empirical parameters r_o and *b* which are established for the given pair of atoms (cation-anion pair) [26]. In this way, it is possible to estimate bond valence sum (BVS, identical to $\sum_j S_{ij}$) value for the chosen ion located at the particular point in the crystal by calculating distances to the neighboring counter-ions. Therefore, bond valence method is readily used to validate a certain structural model and to quantify its stability, through a global instability index GII, which measures the extent to which the bond valence sum rule is violated [27]:

$$GII = \{(\sum_j S_{ij} - V_i)^2\}^{1/2}. \qquad (4)$$

Moreover, based on an assumption that any point in the unit cell having a BVS value for Li^+ close to 1 represents a possible location for Li^+ to be there, BVS distribution on a three-dimensional grid therefore reveals possible locations of Li^+ occurrence in the lattice [17]. Obtained volume for a given BVS mismatch (in this case: 1 ± 0.1 v.u.) represents a 3D map of possible lithium diffusion pathways. For the purposes of this study, bond valence sums were calculated for γ as well as for γ' and ζ structures (structural data of the latter two were taken from literature, Table 2). The BVS calculations performed with the refined γ-LiV_2O_5 structure as input suggest that the conductivity of lithium ions is two-dimensional in the layers perpendicular to c-axis, parallel and in-between of $(V_2O_5)_n$ layers as displayed in Figure 6a. Lithium transfer between the conductive layers is hardly achievable since there are no links of BVS isosurfaces in c-direction. BVS values for the atoms at their refined crystallographic positions are given in Table 2. The global instability index of 0.205 vu implies that a substantial strain is present in the structure, which is at limits of stability [27]. However, the proposed structural model is more stable than the one previously reported in [18] (ICSD #9129). Both insertion and removal of lithium from γ-LiV_2O_5 gives rise to formation of a metastable phases, ζ and γ' respectively, with significantly higher GII values (Table 2). As mentioned earlier, during intercalation in γ phase Li^+ ions are first inserted at Li1 octahedral positions and when all available octahedral sites are taken, Li^+ accommodates at the next available Li2 tetrahedral sites. Both Li1 and Li2 are 4c crystallographic sites with the local *.m.* symmetry [x, ¼, y]. Fractional coordinates of Li1 are given in Table 1, and the fractional coordinates of Li2 are estimated to [0.66, ¼, 0.74]. $Li1O_6$ and $Li2O_4$ polyhedra in the γ-$Li_2V_2O_5$ structure are presented in Figure 6b and their crystal environments are as follows. Assuming 1-electron intercalation (Li2 is thus still unoccupied), each $Li1O_6$ octahedron shares two edges with two neighboring $Li1O_6$, two more edges with two $V1O_5$, two corners with two $V1O_5$ and four corners with four $V2O_5$. On the other hand, each

$Li2O_4$ tetrahedron shares two corners with two $V1O_5$ and one corner with one $L1O_6$, then two edges with two $L1O_6$ and one edge with one $V2O_5$. With insertion of the second lithium in the γ phase the overall number of common edges is thus significantly increased, which generally tends to decrease stability of a structure of ionic crystal [25]. When occupation of available lithium sites (Li1+Li2) reaches ~70%, γ phase transforms to ζ [8,14]. The new ζ phase belongs to the same symmetry group (orthorhombic *Pnma*), but with somewhat different lattice parameters. Most notably, c parameter is shifted towards a lower value: 10.24 Å (ζ) vs. 10.67 Å (γ) [8]. The decrease of c parameter considerably affects electrochemical performance of the ζ-$Li_2V_2O_5$ through the reduction of interlayer spacing (=c/2). Figure 6c and d provide insight into possible diffusion pathways of lithium in the γ and ζ phase, respectively. Although Li1 forms linear chains of edge-shared octahedra along b-direction, the diffusion dominantly takes places through the channels along a-axis intersected with the smaller b-channels at Li2 sites, thus forming 2D diffusion network for γ. In the ζ phase, the a-channels become narrower and b-channels are no longer viable (diffusion of lithium becomes one-dimensional). Most interestingly, the Li2 sites stay completely isolated from the rest of the isosurface area. Therefore, Li2 positions of the ζ phase can be considered as more or less inactive, and all Li^+ found at those sites remain "trapped" once the structure is transformed to ζ. Hence the differences of the charge and discharge voltage profiles, where the charge profile practically lacks Li2 deintercalation region (Figure 4c). Moreover, in this way the material is irreversibly consumed with each new cycle thus resulting in the capacity loss observed at the low voltages. On the opposite side of lithium concentrations, in the high voltage region when γ converts to γ'phase, lithium diffusion undergoes also through a noticeable change of pathways. Still, continuous migration of Li^+ between Li1 sites was granted by the spiral 1D channels along b-axis (Figure 7a, b). The activity of γ' phase therefore remains undisputable.

Table 2. Bond valence sum and global instability index values for γ, γ’ and ζ structure of various compositions.

Atomic position	Bond valence sum (v.u.)					
	γ’-V_2O_5 [4]	γ-LiV_2O_5 [18]	γ-LiV_2O_5 [this work]	γ-$Li_2V_2O_5$ [this work]	ζ-$Li_2V_2O_5$ [8]	ζ-$Li_2V_2O_5$ [14]
Li1	-	0,991	0,936	0,936	0,999	0,978
Li2	-	-	-	1,098	1,163	1,140
V1	5,597	3,821	4,342	4,342	4,581	4,490
V2	5,121	5,300	5,146	4,470	4,685	4,595
O1	-2,154	-2,076	-2,145	-2,455	-2,537	-2,490
O2	-1,839	-1,766	-1,838	-2,052	-2,202	-2,155
O3	-1,862	-1,725	-1,956	-2,124	-2,327	-2,274
O4	-2,415	-2,034	-2,124	-2,146	-2,183	-2,147
O5	-2,448	-2,512	-2,360	-2,069	-2,179	-2,137
GII (v.u.)	0.340	0.255	0.205	0.259	0.385	0.332

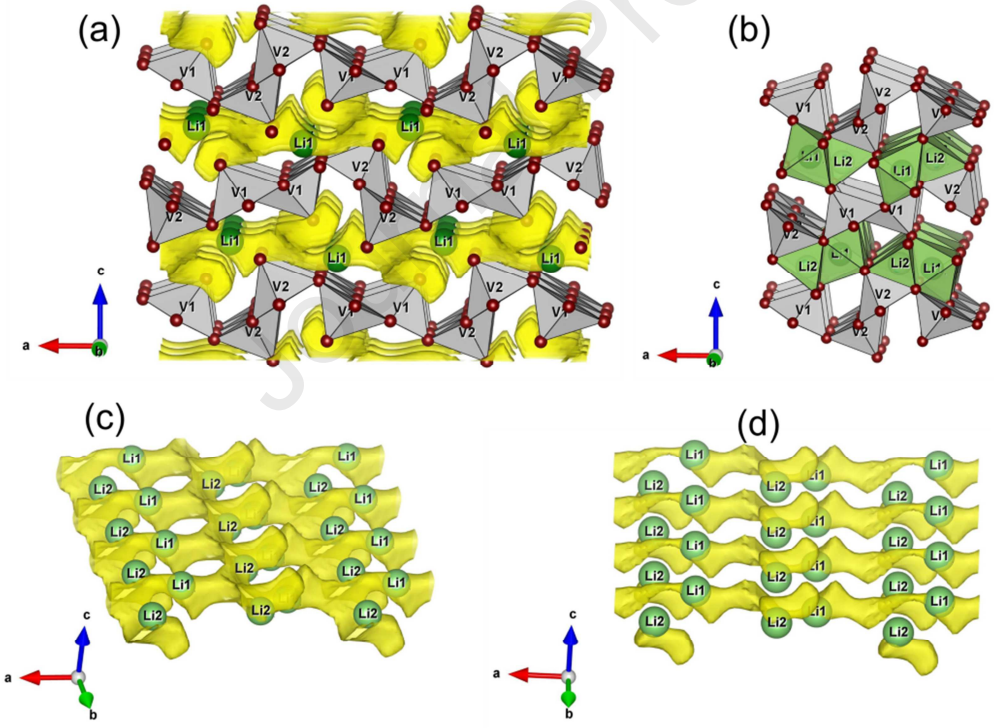

Figure 6. Bond valence model of Li^+ ion migration paths of the γ-LiV_2O_5 (a). Li1 and Li2 positions in the γ-LiV_2O_5 (b). Bond valence model of Li^+ migration in the a-b plane of γ-$Li_2V_2O_5$ (c) and ζ-$Li_2V_2O_5$ (d).

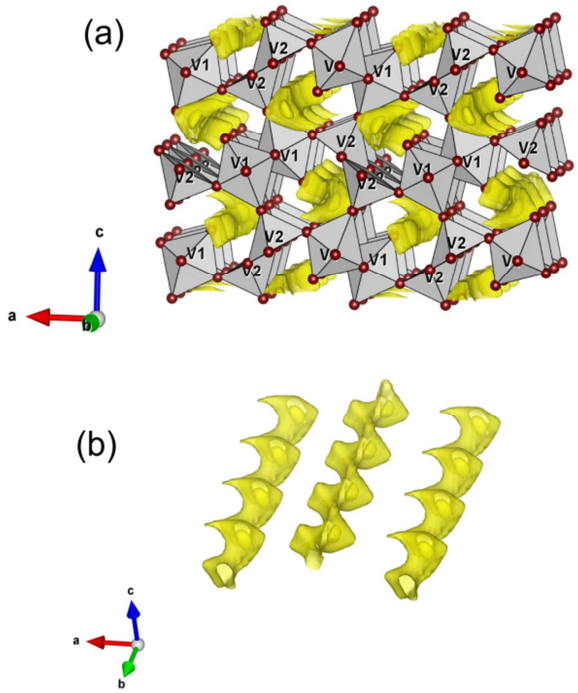

Figure 7. Bond valence model of Li^+ ion migration paths of the γ'-V_2O_5 (a) with 1D diffusion channels along b-direction (b).

4. Conclusion

Lithium vanadium oxide LiV_2O_5 was synthesized via solid state reaction at 700 °C. LiV_2O_5 crystallized as a gamma polymorph γ-LiV_2O_5 and its structure was refined in the orthorhombic space group Pnma. As a candidate for a cathode in the lithium-ion battery, the obtained material was electrochemically examined in an organic electrolyte via galvanostatic charge/discharge tests and in an aqueous electrolyte via cyclic voltammetry measurements. The material exhibited excellent cycling stability in the voltage range from 4 to 3 V vs. Li^+/Li, while in the wider range from 4 to 2.3 V a significant storage capacity loss was observed. The γ structure provides two crystallographic sites to accommodate Li^+, an octahedral Li1 and tetrahedral position Li2. (De)intercalation of lithium in two respective sites occurs at different potentials vs. Li^+/Li: ~3.6V

for Li1 and ~2.4V for Li2 position. By utilizing bond valence method, migration of lithium from these sites was modeled in the γ phase as well as in the metastable phases of lithium poor γ'-V_2O_5 and lithium rich ζ-$Li_2V_2O_5$. γ'-V_2O_5 phase that exists upon complete charge at high voltages, provides continuous network for lithium diffusion between Li1 sites. On the other side, calculated bond valence map of ζ-$Li_2V_2O_5$ suggest the inactivity of lithium at Li2 crystallographic positions is possibly responsible for the stability issues occurring at the low voltages. Therefore, inherent structural characteristics of the ζ phase impede reversible insertion/removal of the second lithium from γ-$Li_xV_2O_5$ system.

Acknowledgements

This research was supported by the Science Fund of the Republic of Serbia, PROMIS, #6062667, HISUPERBAT. The Ministry of Education, Science and Technological Development of the Republic of Serbia provided support under contract # 451-03-68/2020-14/200175. The authors are much obliged to Dr Tanja Barudžija for helpful discussion regarding refinement of crystallite shape and to academician Prof. Dr. Slavko Mentus for providing SEM analysis.

References

[1] M.S. Whittingham, The Role of Ternary Phases in Cathode Reactions, J. Electrochem. Soc. 123 (1976) 315.

[2] J.M. Cocciantelli, J.P. Doumerc, M. Pouchard, M. Broussely, J. Labat, Crystal chemistry of electrochemically inserted $Li_xV_2O_5$, Journal of Power Sources. 34 (1991) 103–111.

[3] C. Delmas, H. Cognac-Auradou, J.M. Cocciantelli, M. Ménétrier, J.P. Doumerc, The $Li_xV_2O_5$ system: An overview of the structure modifications induced by the lithium intercalation, Solid State Ionics. 69 (1994) 257–264.

[4] J.M. Cocciantelli, P. Gravereau, J.P. Doumerc, M. Pouchard, P. Hagenmuller, On the preparation and characterization of a new polymorph of V_2O_5, Journal of Solid State Chemistry. 93 (1991) 497–502.

[5] M. Safrany Renard, N. Emery, R. Baddour-Hadjean, J.-P. Pereira-Ramos, γ'-V_2O_5: A new high voltage cathode material for sodium-ion battery, Electrochimica Acta. 252 (2017) 4–11.

[6] M. Safrany Renard, R. Baddour-Hadjean, J.P. Pereira-Ramos, Kinetic insight into the electrochemical sodium insertion-extraction mechanism of the puckered γ′-V_2O_5 polymorph, Electrochimica Acta. 322 (2019) 134670.

[7] H.G. Bachmann, F.R. Ahmed, W.H. Barnes, The crystal structure of vanadium pentoxide, Zeitschrift Für Kristallographie. 115 (1961) 110–131.

[8] J.M. Coccíantelli, M. Ménétrier, C. Delmas, J.P. Doumerc, M. Pouchard, P. Hagenmuller, Electrochemical and structural characterization of lithium intercalation and deintercalation in the γ-LiV_2O_5 bronze, Solid State Ionics. 50 (1992) 99–105.

[9] J. Barker, M.Y. Saidi, J.L. Swoyer, Performance Evaluation of the Electroactive Material, γ - LiV_2O_5 , Made by a Carbothermal Reduction Method, J. Electrochem. Soc. 150 (2003) A1267.

[10] P. Liu, J.-G. Zhang, J.A. Turner, C.E. Tracy, D.K. Benson, R.N. Bhattacharya, Fabrication of LiV_2O_5 thin-film electrodes for rechargeable lithium batteries, Solid State Ionics. 111 (1998) 145–151.

[11] Y. Wang, Solvothermal synthesis and characterizations of γ-LiV_2O_5 nanorods, Solid State Ionics. 167 (2004) 419–424.

[12] W. Wang, H. Wang, S. Liu, J. Huang, Synthesis of γ-LiV2O5 nanorods as a high-performance cathode for Li ion battery, J Solid State Electrochem. 16 (2012) 2555–2561.

[13] N. Li, H. Gong, Y. Qian, Orthorhombic γ-LiV_2O_5 as Cathode Materials in Lithium Ion Batteries: Synthesis and Property, Chinese Journal of Chemical Physics. 26 (2013) 597–600.

[14] R. Baddour-Hadjean, M. Safrany Renard, J.P. Pereira-Ramos, Unraveling the structural mechanism of Li insertion in γ′-V_2O_5 and its effect on cycling properties, Acta Materialia. 165 (2019) 183–191.

[15] J. Jamnik, J. Maier, Nanocrystallinity effects in lithium battery materials, Physical Chemistry Chemical Physics. 5 (2003) 5215.

[16] T. Roisnel, J. Rodríquez-Carvajal, WinPLOTR: A Windows Tool for Powder Diffraction Pattern Analysis, MSF. 378–381 (2001) 118–123.

[17] M. Sale, M. Avdeev, *3DBVSMAPPER*: a program for automatically generating bond-valence sum landscapes, Journal of Applied Crystallography. 45 (2012) 1054–1056.

[18] D.N. Anderson, R.D. Willett, Refinement of the structure of LiV_2O_5, Acta Cryst B. 27 (1971) 1476–1477.

[19] M. Milović, D. Jugović, N. Cvjetićanin, D. Uskoković, A.S. Milošević, Z.S. Popović, F.R. Vukajlović, Crystal structure analysis and first principle investigation of F doping in $LiFePO_4$, Journal of Power Sources 241 (2013) 70–79.

[20] J. Rodríguez-Carvajal, An introduction to the program FullProf 2000, CEA-CNRS, Gif sur Yvette, FRANCE, 2001.

[21] X. Zhang, R. Frech, Vibrational spectroscopic study of lithium vanadium pentoxides, Electrochimica Acta. 42 (1997) 475–482.

[22] S. Caes, J.C. Arrebola, N. Krins, P. Eloy, E.M. Gaigneaux, C. Henrist, R. Cloots, B. Vertruyen, Mesoporous lithium vanadium oxide as a thin film electrode for lithium-ion

batteries: comparison between direct synthesis of LiV2O5 and electrochemical lithium intercalation in V_2O_5, J. Mater. Chem. A. 2 (2014) 5809–5815.

[23] J. Dai, S.F.Y. Li, Z. Gao, K.S. Siow, Novel Method for Synthesis of γ-Lithium Vanadium Oxide as Cathode Materials in Lithium Ion Batteries, Chem. Mater. 11 (1999) 3086–3090.

[24] A.J. Bard, L.R. Faulkner, Electrochemical methods: fundamentals and applications, 2nd ed, Wiley, New York, 2001.

[25] L. Pauling, The principles determining the structure of complex ionic crystals, J. Am. Chem. Soc. 51 (1929) 1010–1026.

[26] S. Adams, Practical Considerations in Determining Bond Valence Parameters, in: I.D. Brown, K.R. Poeppelmeier (Eds.), Bond Valences, Springer, Berlin, Heidelberg, 2014: pp. 91–128.

[27] I.D. Brown, The chemical bond in inorganic chemistry: the bond valence model, Oxford University Press, Oxford ; New York, 2002.

Declaration of interests

☒ The authors declare that they have no known competing financial interests or personal relationships that could have appeared to influence the work reported in this paper.

☐The authors declare the following financial interests/personal relationships which may be considered as potential competing interests: